



Article

ATP13A2 Regulates Cellular α -Synuclein Multimerization, Membrane Association, and Externalization

Jianmin Si ¹, Chris Van den Haute ^{1,2}, Evy Lobbestael ¹, Shaun Martin ³, Sarah van Veen ³, Peter Vangheluwe ³ and Veerle Baekelandt ^{1,*}

- ¹ Laboratory for Neurobiology and Gene Therapy, Department of Neurosciences, Leuven Brain Institute, KU Leuven, Herestraat 49, Bus 1023, 3000 Leuven, Belgium; jianmin.si@kuleuven.be (J.S.); chris.vandenhaute@kuleuven.be (C.V.d.H.); evy.lobbestael@kuleuven.be (E.L.)
- ² Leuven Viral Vector Core, Division Molecular Medicine, KU Leuven, Herestraat 49, Bus 1023, 3000 Leuven, Belgium
- ³ Laboratory of Cellular Transport Systems, Department of Cellular and Molecular Medicine, KU Leuven, Herestraat 49, Bus 802, 3000 Leuven, Belgium; familyvanmar10@gmail.com (S.M.); sarah.vanveen@kuleuven.be (S.v.V.); peter.vangheluwe@kuleuven.be (P.V.)
- * Correspondence: veerle.baekelandt@kuleuven.be; Tel.: +32-16-374-057

Abstract: ATP13A2, a late endo-/lysosomal polyamine transporter, is implicated in a variety of neurodegenerative diseases, including Parkinson's disease and Kufor-Rakeb syndrome, an early-onset atypical form of parkinsonism. Loss-of-function mutations in ATP13A2 result in lysosomal deficiency as a consequence of impaired lysosomal export of the polyamines spermine/spermidine. Furthermore, accumulating evidence suggests the involvement of ATP13A2 in regulating the fate of α -synuclein, such as cytoplasmic accumulation and external release. However, no consensus has yet been reached on the mechanisms underlying these effects. Here, we aimed to gain more insight into how ATP13A2 is linked to α -synuclein biology in cell models with modified ATP13A2 activity. We found that loss of ATP13A2 impairs lysosomal membrane integrity and induces α -synuclein multimerization at the membrane, which is enhanced in conditions of oxidative stress or exposure to spermine. In contrast, overexpression of ATP13A2 wildtype (WT) had a protective effect on α -synuclein multimerization, which corresponded with reduced α syn membrane association and stimulation of the ubiquitin-proteasome system. We also found that ATP13A2 promoted the secretion of α -synuclein through nanovesicles. Interestingly, the catalytically inactive ATP13A2 D508N mutant also affected polyubiquitination and externalization of α -synuclein multimers, suggesting a regulatory function independent of the ATPase and transport activity. In conclusion, our study demonstrates the impact of ATP13A2 on α -synuclein multimerization via polyamine transport dependent and independent functions.

Keywords: ATP13A2; α -synuclein; α -synuclein multimerization; spermine; Parkinson's disease



Citation: Si, J.; Van den Haute, C.; Lobbestael, E.; Martin, S.; van Veen, S.; Vangheluwe, P.; Baekelandt, V. ATP13A2 Regulates Cellular α -Synuclein Multimerization, Membrane Association, and Externalization. *Int. J. Mol. Sci.* **2021**, *22*, 2689. <https://doi.org/10.3390/ijms22052689>

Academic Editor: Dean L. Pountney

Received: 31 January 2021

Accepted: 2 March 2021

Published: 7 March 2021

Publisher's Note: MDPI stays neutral with regard to jurisdictional claims in published maps and institutional affiliations.



Copyright: © 2021 by the authors. Licensee MDPI, Basel, Switzerland. This article is an open access article distributed under the terms and conditions of the Creative Commons Attribution (CC BY) license (<https://creativecommons.org/licenses/by/4.0/>).

1. Introduction

Parkinson's disease (PD) is the most common neurodegenerative movement disorder, with prominent loss of dopaminergic neurons in the substantia nigra pars compacta (SNpc) and the presence of proteinaceous inclusions termed Lewy bodies [1]. Dopaminergic neuron loss results in the deficiency of dopamine within the basal ganglia and leads to motor dysfunction, such as resting tremor, rigidity, bradykinesia, and postural instability [2]. The main component of the Lewy bodies is α -synuclein (α syn) [3,4]. Both missense mutations (A53T/E, E46K, A30P, H50Q, G51D) and duplication or triplication of the *SNCA* gene (encoding α syn) can cause autosomal dominant PD [5]. In addition, mounting evidence claims that the disruption of various cellular events is mediated by α syn-induced neurotoxicity and suggests that α syn acts as a central player in the pathogenesis of PD [6]. α syn is widely expressed in the central nervous system and is mainly localized in the presynaptic terminals, where it is found both cytosolic and membrane-bound [7,8]. Due to its association

with the synaptic membrane to promote membrane curvature, α syn is strongly suggested as a chaperone protein that regulates the neurotransmitter release [9]. On the other hand, membrane-bound α syn is reported to promote the formation of intracellular aggregates via recruitment of the cytosolic form [10]. Membrane vesicles and lipids have also been reported to accelerate α syn fibrillization by increasing the aggregation kinetics [11]. Additional factors such as oxidation are well known to promote α syn aggregation. Indeed, we previously showed that incubation of neuronal cells with hydrogen peroxidase (H_2O_2) and ferrous chloride ($FeCl_2$) induces α syn aggregation [12]. Moreover, imbalance of α syn synthesis and a progressive decline in proteolytic efficiency can result in abnormal levels of α syn, which will favor the formation of multimers and oligomers, eventually accumulating into toxic fibrillar species [13].

ATP13A2 is a P5B-type ATPase that is highly expressed in the human brain with highest expression in the SNpc [14], where it localizes to lysosomes and late endosomes [15]. Different mutations in the ATP13A2 gene have been shown to be involved in different neurodegenerative diseases including Kufor–Rakeb syndrome, early-onset PD, hereditary spastic paraplegia, neuroid ceroid lipofuscinosis, and amyotrophic lateral sclerosis [16–20]. To date, pathogenic ATP13A2 mutations have been identified that cause a variety of functional deficits, such as subcellular mislocalization, decreased protein half-life, and the loss of protein function [20–22]. Deficiency of ATP13A2 or loss-of-function mutations result in various cellular deficits such as lysosomal impairment, mitochondrial dysfunction, and dyshomeostasis of heavy metals [21–25]. Of interest, α syn and ATP13A2 seem to be members of the same intracellular network. Both deficiency of ATP13A2 and familial ATP13A2 mutations have been reported to directly affect the fate of α syn, such as intracellular accumulation and external release [15,21,26,27]. In addition, a link between ATP13A2 and α syn in the context of PD pathology was supported by the finding that α syn overexpression-induced toxicity in yeast could be rescued by co-expression of the yeast ATP13A2 ortholog YPK9, and dopaminergic neuron loss in *Caenorhabditis elegans* was antagonized by ATP13A2 [28]. Moreover, α syn-induced motor deficits were exacerbated in ATP13A2-deficient mice compared to wildtype (WT) mice [29]. On the other hand, no α syn abnormalities could be observed in ATP13A2-null mice [30] and AAV-mediated overexpression of human ATP13A2 was not protective in an α syn-based rat model of PD [31]. Taken together, the precise mechanism mediating the crosstalk between ATP13A2 and α syn remains poorly understood and requires further research.

We recently reported that ATP13A2 is a lysosomal polyamine exporter with the highest affinity for spermine (SPM) [32]. Polyamines (putrescine, spermidine, and SPM) are involved in many cellular processes, including cell proliferation and differentiation, modulation of ion channels and receptors, and regulation of gene transcription and translation [33]. SPM is an antioxidant under physiological conditions [34], and we recently showed that ATP13A2-mediated SPM transport counteracts mitochondrial oxidative stress [35]. However, at high concentration, SPM exerts toxic effects, possibly due to lysosomal accumulation and lysosomal-dependent cell death [32]. Interestingly, a direct link between spermidine or SPM and α syn aggregation was previously reported, given that polyamines can alter the α syn conformation, making it more prone to aggregation [36,37]. ATP13A2 deficiency sensitizes cells to SPM toxicity, due to impaired lysosomal activity and loss of lysosomal integrity [32]. Since multiple studies demonstrated a relationship between lysosomal dysfunction and α syn aggregation [38], in this study, we wanted to study the effect of ATP13A2 on the pathophysiology of α syn in detail, taking into account these recent findings. We compared basal and stress conditions induced by oxidative stress or SPM and investigated the involvement of ATP13A2 in α syn membrane association and multimerization. In addition, we studied the proteolytic degradation system and exocytosis to determine whether ATP13A2 contributes to the intracellular removal of α syn. We show that knockdown (KD) of ATP13A2 impairs lysosomal membrane integrity, together with increased α syn membrane association and α syn multimerization. Conversely, ATP13A2 WT plays a protective role against α syn multimerization by maintaining the

integrity of the lysosomal membrane and by inhibiting α syn membrane association and multimerization. We also found that it regulates the ubiquitin-proteasome system (UPS) and nanovesicle-based external secretion to remove α syn multimers.

2. Results

2.1. ATP13A2 KD Results in Upregulation of α syn Multimers

Deficiency of ATP13A2 and familial ATP13A2 mutations have been reported to induce α syn aggregation [21,26,28,39]. Here, we aimed to explore effect of ATP13A2 on α syn multimerization. We generated human neuroblastoma SH-SY5Y cells with stable expression of human α syn WT (SH-SY5Y- α syn) combined with microRNA-based short hairpin (sh)-mediated ATP13A2 KD, overexpression of ATP13A2 WT, or overexpression of the ATPase-deficient mutant ATP13A2 D508N (DN). Cell lines expressing sh-firefly luciferase (fLuc) or fLuc were used as a negative control. Comparable overexpression of ATP13A2 WT and DN was confirmed by immunoblotting (Figure A1a, Appendix A). To assess the assembly states of α syn under native conditions, we performed intact cell cross-linking with disuccinimidyl glutarate (DSG), as described before [40]. The reducible crosslinker dithiobis succinimidyl propionate (DSP) was used as a control, given that its interaction with α syn can be cleaved by β -mercaptoethanol. Treatment with 0.5 μ M DSG resulted in the detection of multiple α syn multimers. To ensure physiological levels of cross-linking, we checked DJ-1 dimerization as a positive control and the absence of significant cross-linking of tubulin as a negative control (Figure A1b,c, Appendix A). Comparison of the different cell lines revealed that overexpression of ATP13A2 WT or DN did not significantly affect α syn multimerization under steady-state conditions. However, ATP13A2 KD induced an increase in α syn multimers (Figure 1a,b). No difference could be detected in α syn multimers in control sh-fLuc or fLuc cells (Figure A1d, Appendix A). These findings indicate that deficiency in ATP13A2 increases the presence of α syn multimers under normal conditions.

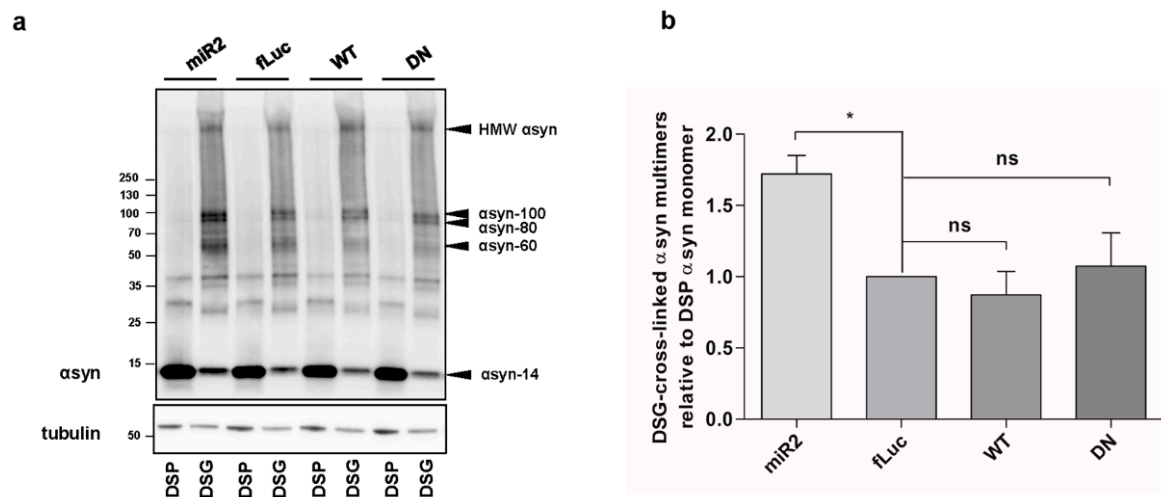


Figure 1. ATP13A2 knockdown (KD) results in upregulation of α syn multimers in SH-SY5Y cells. (a) Visualization of α -synuclein (α syn) multimers by Western blot after cross-linking in ATP13A2 KD, control fLuc, ATP13A2 wildtype (WT), and ATP13A2 D508N (DN) cells. (b) Quantification of disuccinimidyl glutarate (DSG) cross-linked α syn-60 + α syn-80 + α syn-100 + HMW (high molecular weight) α syn relative to dithiobis succinimidyl propionate (DSP) α syn-14 monomer in the ATP13A2 KD, ATP13A2 WT, and ATP13A2 DN cells relative to the ratio in the control cells ($n = 4$). Statistical analysis was performed using a one-way ANOVA test with Bonferroni. The error bars represent the standard error of the mean (SEM). * $p < 0.05$, ns, not significant. α syn-60 = ~60 kDa α syn, α syn-80 = ~80 kDa α syn, α syn-100 = ~100 kDa α syn.

2.2. ATP13A2 Regulates Oxidative Stress-Induced α syn Multimerization

Next, we examined the effect of ATP13A2 on α syn under cellular stress. We previously showed that oxidative Fenton stress caused by FeCl_2 and H_2O_2 induces α syn aggregation [12]. Here, we investigated the impact of Fenton stress on α syn multimerization in cells overexpressing ATP13A2 KD, ATP13A2 WT, or ATP13A2 DN. We confirmed increased α syn multimerization under these conditions using cross-linking (Figure 2a,b or Figure A2a, Appendix A). The oxidative stress-induced α syn multimerization was prevented in conditions of ATP13A2 WT overexpression, but not by the ATPase inactive mutant ATP13A2 DN (Figure 2c,d or Figure A2b, Appendix A).

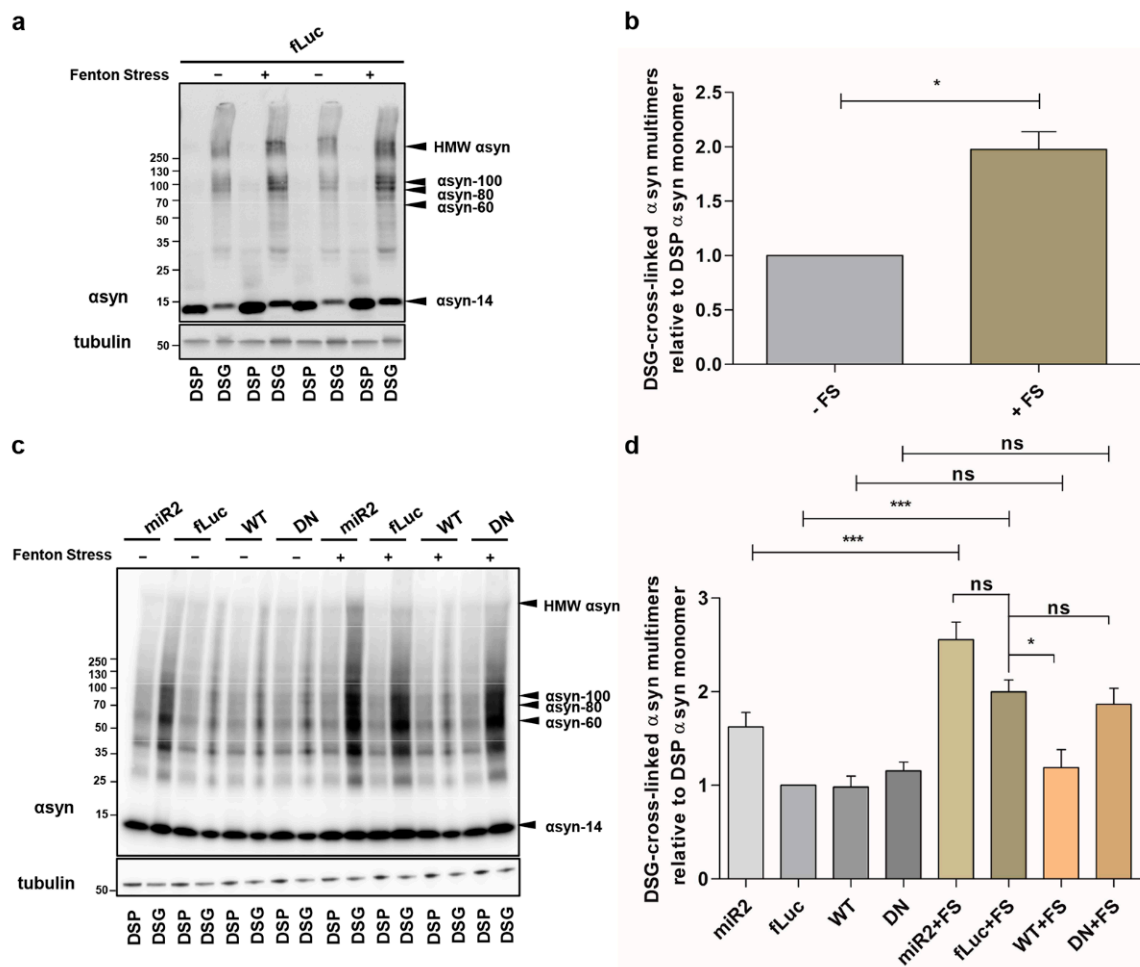


Figure 2. ATP13A2 regulates oxidative stress-induced α syn multimerization. **(a)** Visualization of α syn multimers after cross-linking in control cells without and with oxidative stress. **(b)** Quantification of the α syn multimer-to-monomer ratio relative to the ratio in the control cells ($n = 3$). Statistical analysis was performed with column statistics (one-sample t -test) comparing test values to the hypothetical value of 1. The error bar represents the SEM. * $p < 0.05$. **(c)** Visualization of α syn multimers after cross-linking in ATP13A2 KD, fLuc, ATP13A2 WT, and ATP13A2 DN cells without and with oxidative stress. **(d)** Quantification of the α syn multimer-to-monomer ratio relative to the ratio in the control fLuc cells ($n = 3$). Statistical analysis was performed using a one-way ANOVA test with Bonferroni. The error bars represent the SEM. *** $p < 0.001$, * $p < 0.05$, ns, not significant.

2.3. ATP13A2 Regulates α syn Membrane Association and Multimerization

We further investigated whether ATP13A2 affects the level of membrane-associated α syn since polyamines electrostatically interact with biological membranes to bridge and shield the membrane surface charges that possibly contribute to the aggregation of membrane particles resistant to the repulsive forces [41]. Membrane fractionation experiments revealed that overexpression of ATP13A2 WT reduces α syn levels at the

membrane (Figure 3a,b), while KD of ATP13A2 induced a modest, nonsignificant increase in membrane-associated α syn multimers (Figure 3c,d). We found similar effects in the presence of oxidative stress (Figure 3c,d). To investigate whether increased levels of α syn at the membrane result in increased α syn multimerization, we performed intact cell cross-linking before membrane isolation and assessed the cross-linked α syn multimers in the membrane fraction. In line with the decreased level of membrane-associated α syn, we could observe a reduction of membrane-associated α syn multimers in ATP13A2 WT cells under basal conditions and during oxidative stress (Figure 3e,f). Interestingly, although oxidative stress did not increase the level of membrane-associated α syn, it promoted the multimerization of membrane-associated α syn in ATP13A2 KD, DN and fLuc cells. As in whole-cell extracts, this oxidative stress-induced multimerization at the membrane could also be prevented by ATP13A2 WT overexpression.

2.4. ATP13A2 Inhibits α syn Multimerization via Regulating the UPS

We then wondered whether the observed effect of ATP13A2 WT on α syn multimers was mediated by increased degradation. Therefore, we treated our cells with 10 μ M of the lysosomal inhibitor chloroquine (CQ) for 24 h and found that autophagy inhibition did not affect the level of α syn multimers in ATP13A2 WT cells compared to control conditions (Figure A3a–c, Appendix A). We also explored the involvement of chaperones in the clearance of α syn multimers. We checked the expression levels of Hsc70 and Hsp90 but did not detect significant alterations in conditions with or without oxidative stress in any of the cell lines tested (Figure A3d,e, Appendix A). Next, we investigated the potential role of the UPS, given the previously reported impact of ATP13A2 on polyubiquitination [42]. Oxidative stress induced a significant increase in overall polyubiquitin levels, which was normalized by overexpression of ATP13A2 WT and remarkably ATP13A2 DN (Figure 4a,b). To determine whether this reduced polyubiquitination was related to the clearance of α syn, we treated cells with 1 μ M of the UPS inhibitor MG132 for 24 h and measured the levels of α syn multimers. Inhibition of the UPS did not affect α syn multimerization in basal conditions (Figure A3f, Appendix A). However, during oxidative stress, the protective role of ATP13A2 against α syn multimerization was completely abolished upon UPS inhibition (Figure 4c,d or Figure A3g, Appendix A), pointing to an important role for proteasomal degradation of α syn (multimers) in the observed effect of ATP13A2.

2.5. ATP13A2 Regulates SPM-Induced α syn Multimerization

We recently showed that ATP13A2 is a lysosomal polyamine exporter with the highest affinity for SPM. At high concentrations, polyamines induce cell toxicity, which is exacerbated by ATP13A2 loss due to lysosomal dysfunction and rupture [32]. It was previously reported that SPM can promote α syn aggregation in vitro [43]. Therefore, we investigated whether ATP13A2 influences α syn multimerization in the presence of SPM. We observed that treatment with 5 μ M SPM for 24 h (the concentration was chosen after optimization, considering its toxic effect and the viability of treated cells) induced a twofold increase in α syn multimers in the control fLuc-overexpressing cells. ATP13A2 KD did not significantly enhance α syn multimerization induced by SPM, while overexpression of ATP13A2 WT totally prevented this effect. The ATP13A2 DN cells were similar to the control cells, showing that the protective effect of ATP13A2 WT on SPM-induced α syn multimerization is related to its transport function (Figure 5a,b or Figure A4, Appendix A).

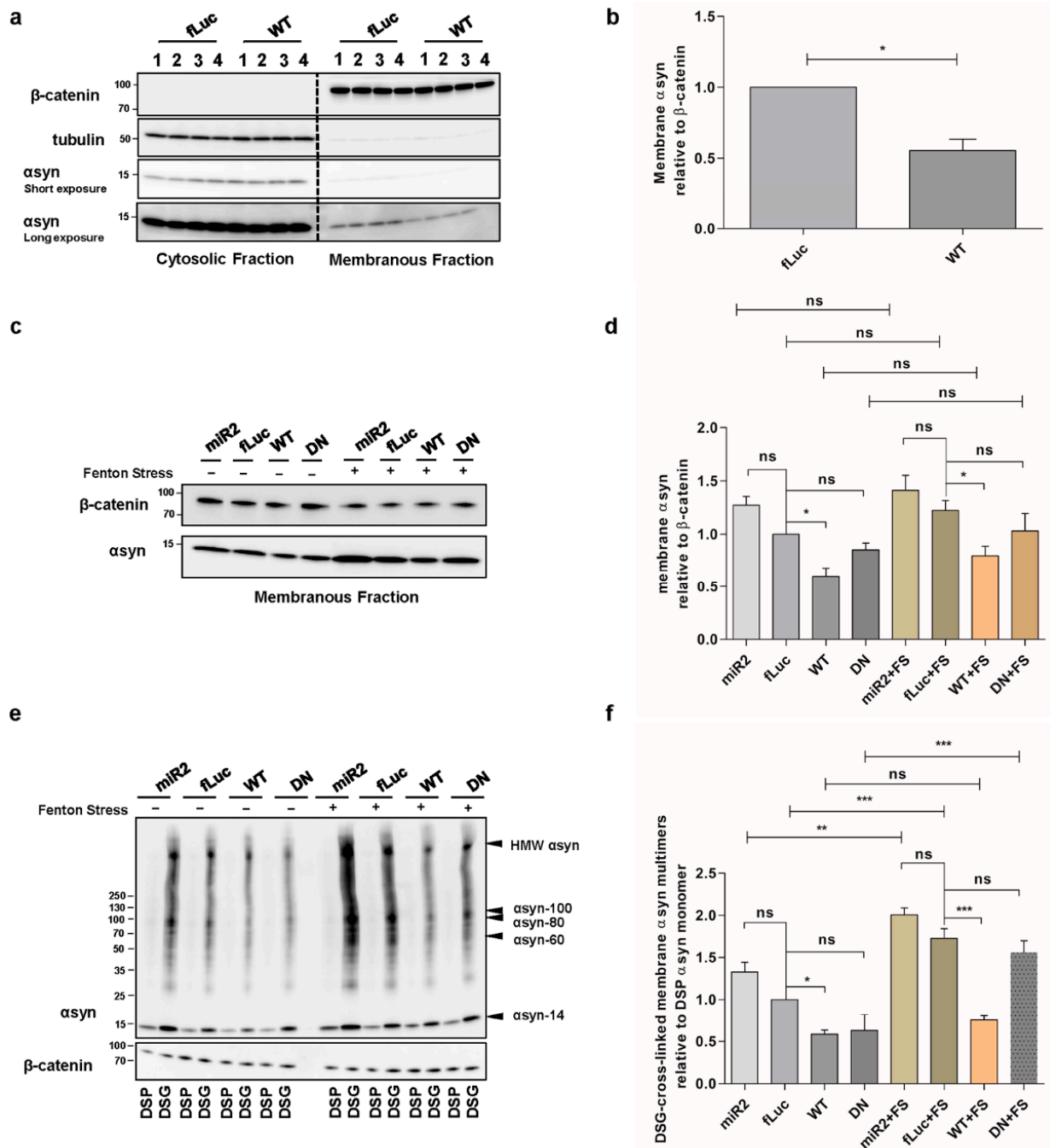


Figure 3. ATP13A2 regulates α syn membrane association and multimerization. (a) Analysis of α syn protein levels by Western blot in the cytosolic and membrane fraction of control and ATP13A2 WT cells using β -catenin as a marker for the membrane fraction and tubulin as a marker for the cytosolic fraction. (b) Quantification of membrane-associated α syn relative to β -catenin ($n = 3$). Statistical analysis was performed with column statistics (one-sample t -test) comparing test values to the hypothetical value of 1. The error bars represent the SEM. * $p < 0.05$. (c) Analysis of α syn protein levels in the membrane fraction of ATP13A2 KD, control, ATP13A2 WT, and ATP13A2 DN cells without and with oxidative stress by Western blot using β -catenin as a standard. (d) Quantification of membrane-associated α syn relative to β -catenin ($n = 3$). Statistical analysis was performed using a one-way ANOVA test with Bonferroni. The error bars represent the SEM. * $p < 0.05$, ns, not significant. (e) Cell lysates of cross-linked membrane fractions from ATP13A2 KD, control, ATP13A2 WT, and ATP13A2 DN cells without and with oxidative stress. (f) Quantification of ratio of membrane-associated α syn multimers to DSP- α syn. Statistical analysis was performed using a one-way ANOVA test with Bonferroni. The error bars represent the SEM. *** $p < 0.001$, ** $p < 0.01$, * $p < 0.05$, ns, not significant.

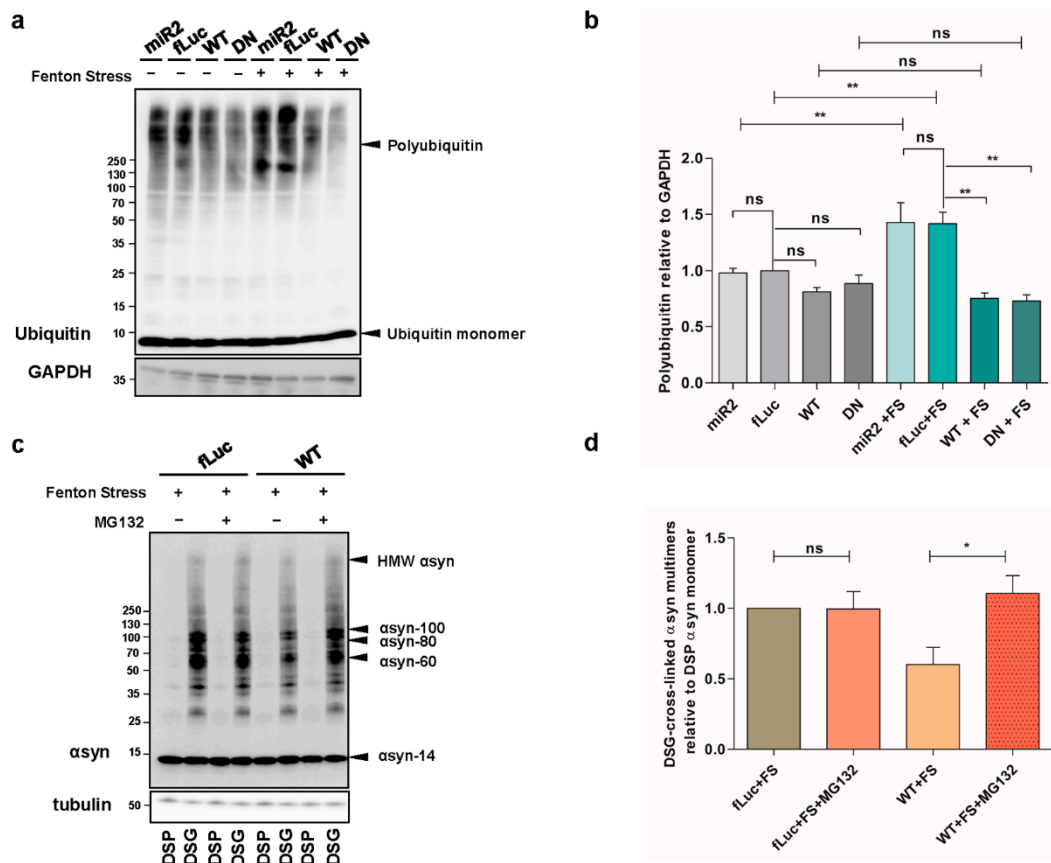


Figure 4. ATP13A2 inhibits α syn multimerization via regulating the ubiquitin-proteasome system (UPS). (a) Visualization of ubiquitin levels in cell lysates from ATP13A2 KD, fLuc, ATP13A2 WT, and ATP13A2 DN cells without and with oxidative stress treatment. Glyceraldehyde 3-phosphate dehydrogenase (GAPDH) levels were used as standard. (b) Quantification of polyubiquitin levels relative to glyceraldehyde 3-phosphate dehydrogenase (GAPDH) ($n = 4$). Statistical analysis was performed using a one-way ANOVA test with Bonferroni. The error bars represent the SEM. ** $p < 0.01$, ns, not significant. (c) Visualization of α syn multimers after cross-linking in fLuc and ATP13A2 WT cells under oxidative stress without and with 1 μ M MG132. (d) Quantification of α syn multimer-to-monomer ratio ($n = 4$). Statistical analysis was performed with column statistics (one-sample t -test) comparing test values to the hypothetical value of 1. * $p < 0.05$, ns, not significant.

Interestingly, while treatment with SPM did not affect α syn levels at the membrane (Figure 5c,d), it resulted in significantly more membrane-bound α syn in the membrane fraction in ATP13A2 KD cells (Figure 5e,f). When considering membrane-associated α syn multimers, SPM challenge further enhanced the increase in ATP13A2 KD cells, which was again prevented by ATP13A2 WT overexpression but not DN (Figure 5e,f).

2.6. Impaired Lysosomal Membrane Integrity Is Linked to α syn Multimerization

We previously reported that high concentrations of SPM induce the loss of lysosomal membrane integrity in ATP13A2 knockout (KO) cells [32]. Here, we aimed to link these findings to α syn multimerization. To this end, we used acridine orange to detect the integrity of the lysosomes. Acridine orange is a weak base dye that becomes protonated under acidic conditions and gets trapped in lysosomes. However, if the lysosomal membrane is damaged, it can diffuse to the cytoplasm, where it gets deprotonated and shifts its emission from red to green fluorescence. We first compared the different α syn expressing cell lines and found that the lysosomal membrane integrity was impaired in ATP13A2 KD cells in basal conditions, while overexpression of ATP13A2 WT or DN had no effect (Figure 6a), which is in line with previous findings [32]. We also validated the acridine orange assay by exposure of the cell lines to high concentration of chloroquine (500 μ M, 2 h), which induces acute impairment of the lysosomal membrane (Figure 6b). Next, we observed that SPM

treatment resulted in a greater loss of lysosomal membrane integrity only when ATP13A2 levels were reduced (Figure 6c). Therefore, we independently confirmed the essential role for ATP13A2 in maintaining the integrity of the lysosomal membrane during SPM-induced stress in a new cell model.

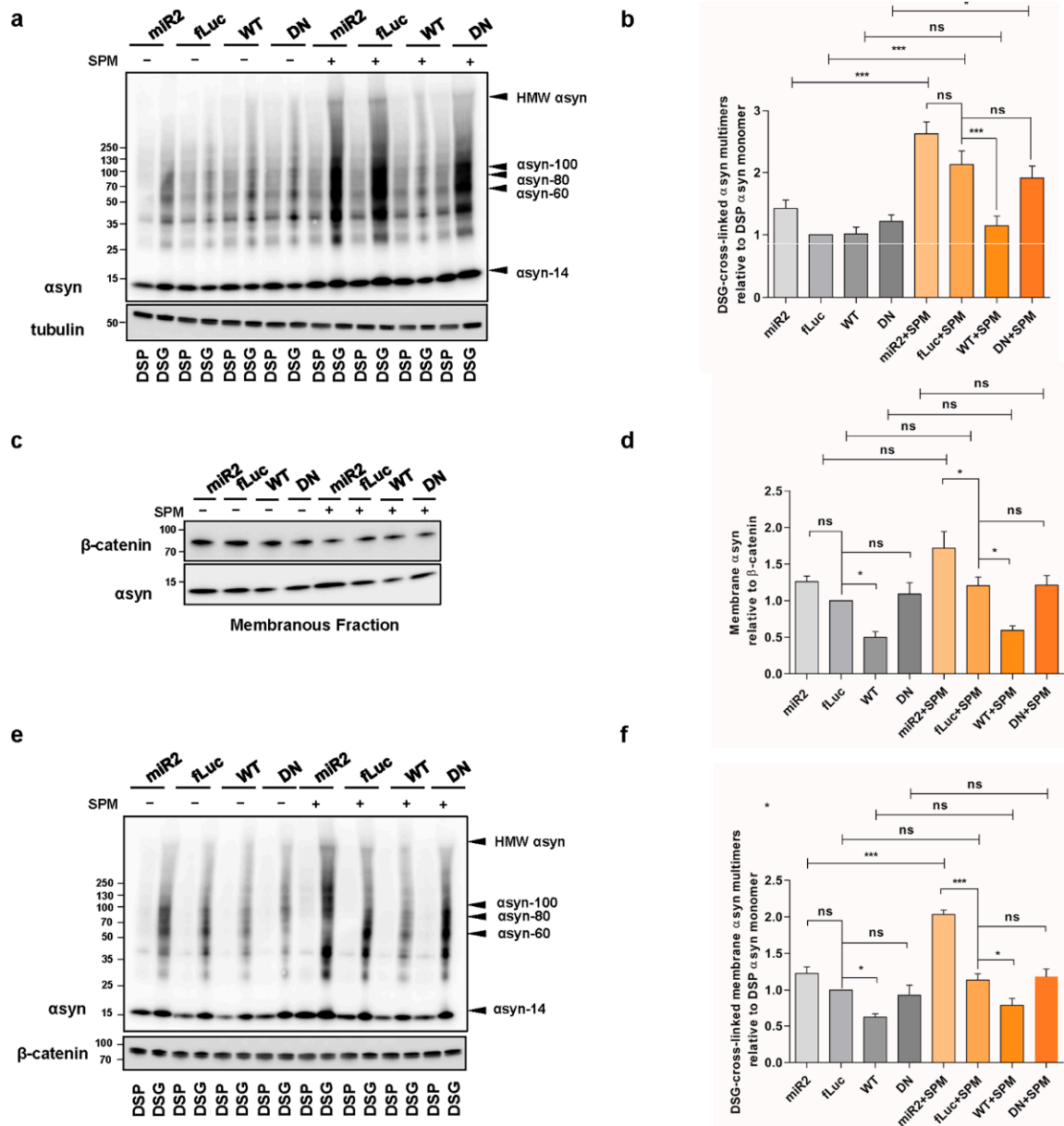


Figure 5. ATP13A2 regulates SPM-induced α syn multimerization. (a) Visualization of α syn multimers after cross-linking in ATP13A2 KD, control, ATP13A2 WT, and ATP13A2 DN cells without and with SPM treatment. (b) Quantification of the α syn multimer-to-monomer ratio relative to the ratio in the control cells ($n = 3$). Statistical analysis was performed using a one-way ANOVA test with Bonferroni. The error bar represents the SEM. *** $p < 0.001$, * $p < 0.05$, ns, not significant. (c) Visualization of α syn protein levels in the membrane fraction of ATP13A2 KD, control, ATP13A2 WT, and ATP13A2 DN cells without and with SPM treatment were analyzed by Western blot using β -catenin as a standard. (d) Quantification of membrane-associated α syn relative to β -catenin ($n = 3$). Statistical analysis was performed using a one-way ANOVA test with Bonferroni. The error bars represent the SEM. * $p < 0.05$, ns, not significant. (e) Visualization of α syn multimers after cross-linking in membrane fraction from ATP13A2 KD, fLuc, ATP13A2 WT, and ATP13A2 DN cells without and with oxidative stress. (f) Quantification of ratio of membrane-associated α syn multimers to DSP- α syn monomer ($n = 3$). Statistical analysis was performed using a one-way ANOVA test with Bonferroni. The error bars represent the SEM. *** $p < 0.001$, * $p < 0.05$, ns, not significant.

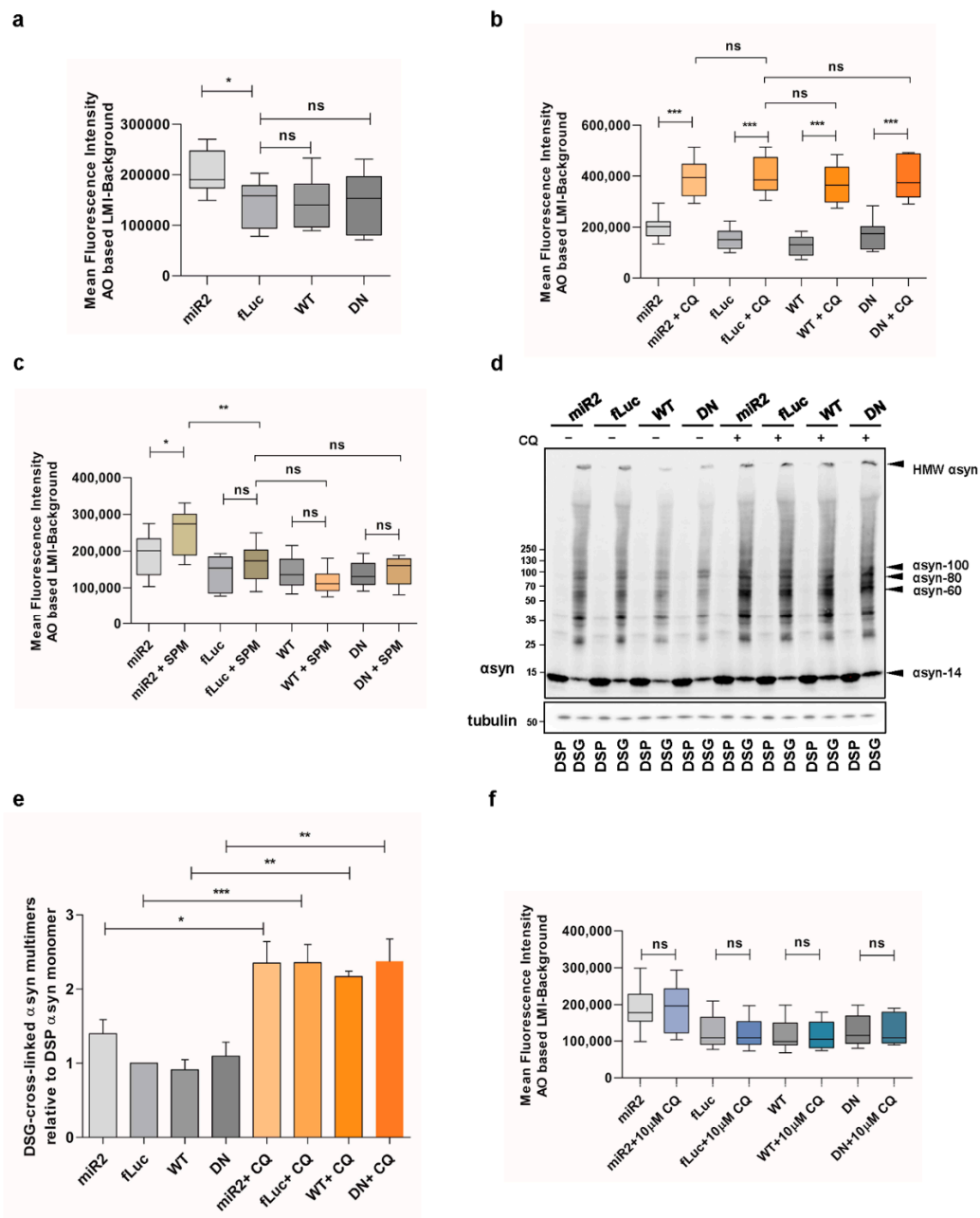


Figure 6. Impaired lysosomal membrane integrity is linked to α syn multimerization. (a) Assessment of lysosomal membrane integrity via acridine orange staining in basal conditions ($n = 9$). Statistical analysis was performed using a one-way ANOVA test with Bonferroni. The error bars represent the SEM. * $p < 0.05$, ns, not significant. AO = acridine orange, LMI = lysosomal membrane integrity. (b) Assessment of lysosomal membrane integrity via acridine orange staining in ATP13A2 KD, fLuc, ATP13A2 WT, and ATP13A2 DN cells without and with chloroquine (CQ) ($n = 9$). Statistical analysis was performed using a one-way ANOVA test with Bonferroni. The error bars represent the SEM. *** $p < 0.001$, ns, not significant. (c) Assessment of lysosomal membrane integrity via acridine orange staining in ATP13A2 KD, fLuc, ATP13A2 WT, and ATP13A2 DN cells without and with SPM ($n = 9$). Statistical analysis was performed using a one-way ANOVA test with Bonferroni. The error bars represent the SEM. ** $p < 0.01$, * $p < 0.05$, ns, not significant. (d) Visualization of α syn multimers after cross-linking in control cells without and with a high concentration of CQ. (e) Quantification of the α syn multimer-to-monomer ratio relative to the ratio in the control cells ($n = 3$). Statistical analysis was performed using a one-way ANOVA test with Bonferroni. The error bars represent the SEM. *** $p < 0.001$, ** $p < 0.01$, * $p < 0.05$. (f) Assessment of lysosomal membrane integrity via acridine orange staining in ATP13A2 KD, fLuc, ATP13A2 WT, and ATP13A2 DN cells without and with a low concentration of CQ ($n = 9$). Statistical analysis was performed using a one-way ANOVA test with Bonferroni. The error bars represent the SEM. ns, not significant.

Of note, high CQ concentrations also induced a pronounced increase of α syn multimers independent of ATP13A2 (Figure 6d,e or Figure A5, Appendix A), while low concentrations of CQ had no effect on α syn multimerization both in basal and oxidative stress condition (Figure A3b,c, Appendix A). Thereafter, we studied the integrity of lysosomal membrane following the challenge with 10 μ M CQ for 24h and confirmed that low concentrations of CQ are not sufficient to induce the damage of lysosomal membranes (Figure 6f), demonstrating that stress-induced lysosomal membrane damage may be linked to α syn multimerization.

2.7. ATP13A2 Promotes Secretion of α syn Multimers

Spreading of aggregated α syn is considered as a key event in PD progression. Since ATP13A2 was reported to regulate the biogenesis of exosomes and promote α syn secretion [15,27], we aimed to determine whether this effect relies on the ATPase function of ATP13A2. Therefore, we set out to investigate the level of extracellular α syn carried by nanovesicles derived from the plasma membrane in our different cell models. By loading the same concentration of nanovesicle proteins, we found that overexpression of ATP13A2 WT and transport-deficient mutant ATP13A2 DN significantly increases the level of α syn in nanovesicles (Figure 7a,b), suggesting that α syn externalization is regulated by ATP13A2 via transport independent roles. Next, we performed cross-linking on the harvested intact nanovesicles to assess the level of α syn multimerization in the secreted nanovesicles. We found that secretion of α syn multimers was promoted by ATP13A2 WT and DN, while ATP13A2 KD did not have any significant effect. Treatment with SPM did not affect the secretion of α syn multimers in any of the cell lines in line with the transport-independent effect of ATP13A2 on nanovesicle secretion, further indicating that nanovesicle secretion is not affected by lysosomal dysfunction (Figure 7c,d). Collectively, these data suggest that ATP13A2 can promote extracellular secretion of α syn multimers through a transport-independent mechanism.

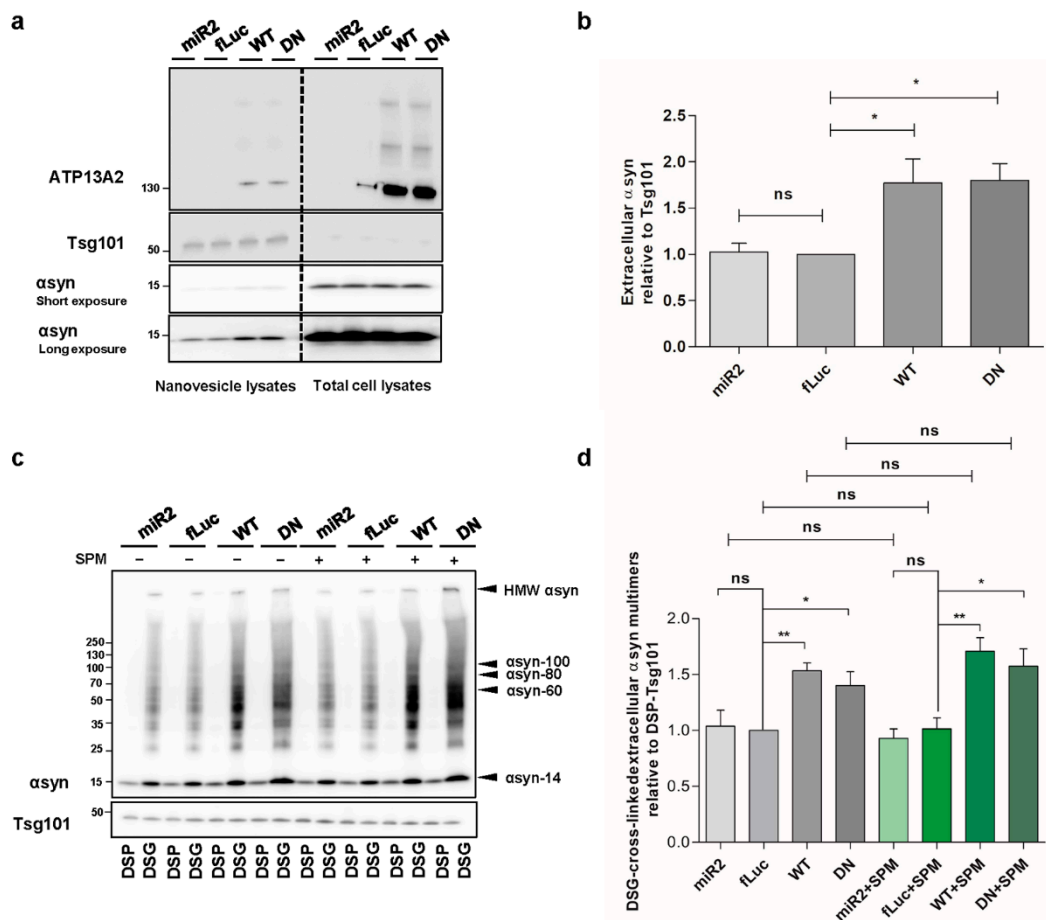


Figure 7. ATP13A2 promotes secretion of α syn multimers. (a) Visualization of α syn protein levels in total cell lysates and nanovesicle extracts from ATP13A2 KD, control, ATP13A2 WT, and ATP13A2 DN cells using Tsg101 as a control for the nanovesicle fraction. (b) Quantification of α syn relative to Tsg101 ($n = 3$). Statistical analysis was performed using a one-way ANOVA test with Bonferroni. The error bars represent the SEM. * $p < 0.05$, ns, not significant. (c) Visualization of α syn multimers after cross-linking in nanovesicles from ATP13A2 KD, control, and ATP13A2 DN cells without and with SPM using Tsg101 as a control for the nanovesicle fraction. (d) Quantification of ratio of α syn multimers to DSP-Tsg101. Statistical analysis was performed using a one-way ANOVA test with Bonferroni. The error bars represent the SEM. ** $p < 0.01$, * $p < 0.05$, ns, not significant.

3. Discussion

In this study, we investigated in detail the relationship between ATP13A2 and α syn multimerization, membrane localization, and secretion in basal conditions compared to conditions of oxidative stress and lysosomal rupture. Despite several previous studies having already considered the potential link between ATP13A2 and α syn, such as those showing that deficiency of ATP13A2 leads to α syn accumulation, as well as the protective effect of ATP13A2 against α syn-induced neurotoxicity [21,22,28], the exact mechanisms underlying these effects remain incompletely resolved.

Our recent identification of SPM as a substrate of ATP13A2 sheds new light on the link between ATP13A2 and α syn [32]. Polyamines enter the cells via endocytosis and, therefore, arrive in the lysosome. Since ATP13A2 functions as an SPM exporter in the lysosomal membrane, loss of ATP13A2 results in increased SPM trapped in the lysosomes, which leads to an overall lower polyamine content in cells. The accumulation of polyamines in the lysosome can ultimately cause lysosomal dysfunction and membrane rupture. We show that SPM exposure reduces lysosomal membrane integrity in our ATP13A2-deficient α syn-expressing cells. Thus, lysosomal dysfunction and loss of lysosomal membrane integrity

may, therefore, at least be partially responsible for the increased α syn multimerization in ATP13A2-deficient cells.

We also found that deficiency in ATP13A2 increases α syn multimerization in basal conditions. The levels of α syn multimers induced by oxidative stress or SPM were increased in conditions of ATP13A2 KD and could be completely prevented upon overexpression of ATP13A2 WT, but not by the transport-deficient mutant DN. This is an interesting finding given the high oxidative stress levels in PD brain and highlights the importance of ATP13A2 in the prevention of α syn multimerization in conditions of oxidative stress.

Under physiological conditions, α syn populates an ensemble of conformations by interacting with proteins or binding to membranes, mediating a variety of cellular events [9], whereas membrane-associated α syn can also disrupt the lipid bilayer and induce pore-like structures, thereby accelerating α syn aggregation [10,44,45]. Here, we found that reduced ATP13A2 levels result in increased levels of α syn multimers at the membrane in conditions of oxidative stress or upon SPM treatment. Conversely, ATP13A2 WT prevents membrane α syn multimerization in these stress conditions. Thus, ATP13A2 may regulate the levels of α syn associated with the membrane, thereby controlling α syn multimerization.

KD or KO of ATP13A2 may result in impaired autophagy, which has been linked to α syn accumulation [21,46]. However, here, we first observed that increased overall polyubiquitin levels can be normalized by ATP13A2 WT and DN, suggesting that ATP13A2 can reduce polyubiquitination or promote degradation of polyubiquitinated proteins in a transport-independent manner, which is in line with previous findings [42]. Next, we found that inhibition of the ubiquitin-proteasome system but not the autophagy lysosomal pathway blocked the protective role of ATP13A2 against α syn multimerization. This might indicate that ATP13A2-mediated removal of α syn multimers occurs through the UPS in the conditions tested.

Spreading of pathological α syn contributes to the neurodegenerative phenotype in a number of cell and animal models. Previous studies suggested the involvement of ATP13A2 in the biogenesis of exosomes and α syn externalization [15,27], but the role of the transport function of ATP13A2 was not addressed. For this phenotype, we found that, independent of the transport function, ATP13A2 significantly increases the level of α syn carried by nanovesicles, while ATP13A2 KD did not have any significant effect. In addition, by loading the same volume of nanovesicle samples from different cells, we also confirmed that ATP13A2 WT and DN can increase the biogenesis of exosomes, and that ATP13A2 KD seems to correlate with decreased level of exosome markers, which is in line with previous findings (Figure A6) [27]. These are interesting findings suggesting that ATP13A2 might be able to promote the sequestration of α syn, which is subsequently externalized through nanovesicles. Moreover, when examined which α syn species are externalized, strikingly, we found that, independent of the transport function, ATP13A2 significantly increases the release of α syn multimers via nanovesicles. This is an intriguing finding, since one could argue that increased release of (multimeric) α syn reduces the cellular α syn levels but might at the same time promote the spreading of extracellular α syn, thus amplifying the progression of the toxic effect from neurons to surrounding tissues. Thus, further studies will be required to determine whether these α syn multimers in the nanovesicles are related to pathological spread in vivo or rather to a way for the cell to reduce its levels of α syn (multimers) without detrimental effects on neighboring cells.

We used the artificial, transport-deficient mutant ATP13A2 DN as a control in several of our experiments, which enabled us to dissect polyamine transport-dependent and -independent functions of ATP13A2 [32]. ATP13A2 DN did not show significant effects in most conditions tested; however, it could prevent increased polyubiquitination induced via oxidative stress, as well as promote the externalization of α syn multimers. Taken together, these findings suggest a scaffolding function of ATP13A2 next to the transporter role, which is in accordance with previous reports [42].

4. Materials and Methods

4.1. Generation of Stable Overexpression Cell Lines

Human neuroblastoma SH-SY5Y cells with stable expression of human α syn WT were generated using pCHMWS- α syn-IRES-puro lentiviral vectors (LVs), and cells were selected with puromycin (3 μ g/mL, Gibco, Gaithersburg, MD, USA). Next, these selected cells were transduced with human ATP13A2-WT-IRES-puromycin, human ATP13A2-D508N-IRES-puromycin, fLuc-IRES-puromycin (control), sh-ATP13A2-blasticidin (KD), and sh-fLuc-blasticidin (KD control) LVs to obtain ATP13A2 overexpression or KD cells. All LVs were generated by the Leuven Viral Vector Core (LVVC) as described previously [42,47]. Cells were grown as monolayers and maintained in Dulbecco's modified Eagle's medium (DMEM) with Glutamax (Gibco, Gaithersburg, MD, USA), supplemented with 15% fetal calf serum (FCS; Gibco, Gaithersburg, MD, USA), 1% nonessential amino acids (NEAAs; Gibco, Gaithersburg, MD, USA), and gentamicin (50 μ g/mL; Gibco, Gaithersburg, MD, USA) at 37 °C in a humidified atmosphere containing 5% CO₂. After lentiviral transduction, cells were selected with blasticidin (9 μ g/mL, Thermo Fisher Scientific, Waltham, MA, USA) or puromycin (3 μ g/mL). To inhibit proteasomal or lysosomal activity, cells were treated for 24 h with 1 μ M MG132 (Sigma-Aldrich, Saint Louis, MO, USA) or 10 μ M chloroquine (CQ, Sigma-Aldrich, Saint Louis, MO, USA), respectively. For cell lysis, cells were washed with phosphate-buffered saline (PBS) and lysed in lysis buffer (Tris 20 mM pH 7.5, NaCl 150 mM, ethylenediaminetetraacetic acid (EDTA) 1 mM, Triton 1%, glycerol 10%, and protease inhibitor (PI) cocktail (Roche, Basel, Switzerland)). Cell lysates were cleared by centrifugation at 12,000 \times g for 15 min and further analyzed via immunoblotting.

4.2. Oxidative Stress Cell Model and SPM Addition

To induce α syn aggregation, oxidative stress was applied to the cells as described by Macchi et al. with a few modifications [12]. One day after plating the cells in 10 cm dishes, cells were treated with 5 mM freshly prepared FeCl₂ (Sigma-Aldrich, Saint Louis, MO, USA) and 100 μ M H₂O₂ (Sigma-Aldrich, Saint Louis, MO, USA) in DMEM-complete (filtered through a 0.45 μ m filter (Merck Millipore, Burlington, MA, USA)). After 72 h, cells were washed with PBS and scraped for immunoblotting or intact cell cross-linking.

SPM (Sigma-Aldrich, Saint Louis, MO, USA) was prepared to a final stock concentration of 200 mM in 0.1 M 3-(N-morpholino)propane sulfonic acid (MOPS)-KOH (pH 7.0) [32]. For the SPM assay, cells were treated with 10 μ M freshly prepared SPM for 24 h; then, cells were washed with PBS and scraped for intact cell cross-linking.

4.3. Intact Cell Cross-Linking

Cells were washed twice with PBS and harvested with PBS with PI cocktail (PBS + PI buffer). After centrifuging at 1000 \times g for 15 min, the cells were resuspended in 200 μ L of PBS + PI buffer. Next, we incubated the cells with 0.5 μ M DSG (Thermo Fisher Scientific, Waltham, MA, USA) or 1 μ M DSP (Thermo Fisher Scientific, Waltham, MA, USA) for 30 min at 37 °C. The reaction was quenched with 10 μ L of Tris-HCl buffer (1 M, pH 7.4) for 15 min at room temperature. Then cells were sonicated twice at 30 Hz for 15 on-off intervals of 10 s each (1 s pulse on/off) (Branson Sonifier, Ede, Netherlands).

4.4. Membrane Fractionation

Cells were washed twice with PBS, scraped, and harvested with PBS + PI buffer. After centrifuging at 1000 \times g for 15 min, the cells were resuspended in 500 μ L of PBS + PI buffer and sonicated twice at 30 Hz for 15 on-off intervals of 10 s each (1 s pulse on/off). After sonication, cells were centrifuged at 340,000 \times g at 4 °C for 15 min, and the supernatant was collected as the cytosolic fraction. The pellets were washed three times with PBS + PI buffer and centrifuged at 340,000 \times g for 15 min; then, the pellets were dissolved in PBS + PI + 1% Triton buffer. After centrifugation at 340,000 \times g at 4 °C for 15 min, the supernatant was collected as membranous fraction. For intact cell cross-linking

combined with membrane fractionation experiments, cells were treated with cross-linker first, followed by membrane fractionation.

4.5. Nanovesicle Isolation

Cells were plated in 3×15 cm dishes and allowed to attach overnight. The next day, the cells were washed twice with PBS, and DMEM with 1% exosome-depleted fetal bovine serum (FBS) was added to each plate. The medium was collected 24 h later, and nanovesicles were purified using differential centrifugation: $300 \times g$ for 15 min to remove cells, $15,000 \times g$ for 30 min to remove cell debris, filtration of apoptotic bodies through a $0.22 \mu\text{m}$ filter, and a final spin at $140,000 \times g$ for 3 h at 4°C . Supernatant was decanted, and nanovesicles were collected in $50 \mu\text{L}$ of cell lysis buffer for immunoblotting. For intact nanovesicle cross-linking, 9×15 cm dishes cells were plated. The nanovesicles were dissolved in $200 \mu\text{L}$ of PBS + PI buffer, followed by cross-linking with DSP or DSG.

4.6. Lysosomal Membrane Integrity

To assess lysosomal membrane integrity, cells were seeded in 12-well plates; the next day, cells were incubated with $5 \mu\text{g}/\text{mL}$ acridine orange (dissolved in media, Thermo Scientific, Waltham, MA, USA) for 15 min at 37°C . Thereafter, medium was discarded, cells were washed with PBS, and fresh medium was added. Then, cells were treated with the indicated concentrations of SPM or the positive control chloroquine ($500 \mu\text{M}$) for 2 h at 37°C . Lastly, cells were collected and resuspended in PBS containing 1% bovine serum albumin (BSA). The mean fluorescence of 10,000 events was captured using an Attune Nxt (Thermo Scientific, Waltham, MA, USA) flow cytometer.

4.7. Immunoblotting

After determination of protein content using a bicinchoninic acid (BCA) assay (Pierce Biotechnology, Waltham, MA, USA), cell extracts containing $15 \mu\text{g}$ of total protein were separated on 4–15% precast midi protein gels (Bio-Rad, Hercules, CA, USA) and electroblotted onto polyvinylidene difluoride membranes (Bio-Rad, Hercules, CA, USA). Membranes were first incubated with 0.4% paraformaldehyde (PFA) for 15 min for better αsyn binding, then blocked with PBST with 5% milk for 30 min and incubated with the following primary antibodies: anti- $\alpha\text{-Syn}$ (BD Transduction, San Jose, CA, USA), anti- $\alpha\text{-tubulin}$ (Sigma-Aldrich, Saint Louis, MO, USA), anti-ubiquitin (Abcam, Cambridge, MA, USA), anti-GAPDH (Abcam, Cambridge, MA, USA), anti- $\beta\text{-catenin}$ (Abcam, Cambridge, MA, USA), anti-Hsc70 (Abcam, Cambridge, MA, USA), anti-Hsp90 (Abcam, Cambridge, MA, USA), anti-LC3 (Novus Biologicals, Centennial, CO, USA), and anti-ATP13A2 (Sigma-Aldrich, Saint Louis, MO, USA). After overnight incubation with primary antibodies at 4°C , blots were washed three times with PBS/1%Triton and incubated with horseradish peroxidase-conjugated secondary antibodies (Dako, Glostrup, Denmark) for 1 h. Detection was performed using chemiluminescence (Thermo Fisher Scientific, Waltham, MA, USA) and an LAS-4000 imaging system (Fujifilm, Saitama, Japan).

4.8. Statistics

Figures shown are representative of at least three independent experiments. Images were analyzed by ImageJ 1.49v, and data were analyzed using Graph Pad Prism 6 (version 6.00, GraphPad Software, San Diego, CA, USA). Statistical analysis was performed using a one-way ANOVA test with Bonferroni to compare selected pairs of columns or column statistics (one-sample *t*-test) to compare values to the hypothetical value of 1. All error bars represent the standard error of the mean (SEM). Statistical significance was set at *** $p < 0.001$, ** $p < 0.01$, and * $p < 0.05$.

5. Conclusions

Our findings indicate that ATP13A2 regulates αsyn multimerization induced by oxidative stress or SPM via a mechanism involving maintenance of lysosomal membrane

integrity, regulation of α syn membrane association, and UPS-mediated α syn degradation. Our findings shed new light on the link between α syn and ATP13A2 and provide an explanation for the protective role of ATP13A2.

Author Contributions: Conceptualization, P.V. and V.B.; methodology, J.S., S.v.V. and S.M.; software, J.S., E.L., and C.V.d.H.; validation, J.S.; formal analysis, J.S.; investigation, J.S.; writing—original draft preparation, J.S.; writing—review and editing, C.V.d.H., E.L., S.M., P.V., and V.B.; supervision, C.V.d.H., E.L., and V.B.; project administration, V.B.; funding acquisition, V.B. All authors read and agreed to the published version of the manuscript.

Funding: This work was supported by the FWO Flanders (Projects G.0927.14, G080517N, and SBO S006617N Neuro-TRAFFIC, postdoctoral fellowship to S.v.V.), the KU Leuven (OT/14/120, C14/18/102, DBOF fellowship to Jianmin Si), the ERA-NET JPco-fuND 2015 SYNACTION (JPND-SYNACTION-ANR-15-JPWG-0012-03), the Medical Foundation Queen Elisabeth and joint efforts of the Michael J. Fox Foundation for Parkinson’s Research (MJFF) and the Aligning Science Across Parkinson’s (ASAP) initiative Grant-ID ASAP-000458 IMPACT-PD.

Institutional Review Board Statement: Not applicable.

Informed Consent Statement: Not applicable.

Data Availability Statement: All data are reported in the manuscript and in the Appendix A.

Acknowledgments: We thank J.V. Asselbergs for his technical assistance and the Leuven Viral Vector Core (LVVC) for the viral vector production. S.M. and S.v.V. helped with the lysosomal assays. Membrane fractionation and nanovesicle isolation were performed in the CMM ultracentrifugation park at KU Leuven, supported by S.M. and S.v.V.

Conflicts of Interest: The authors declare no conflict of interest.

Appendix A

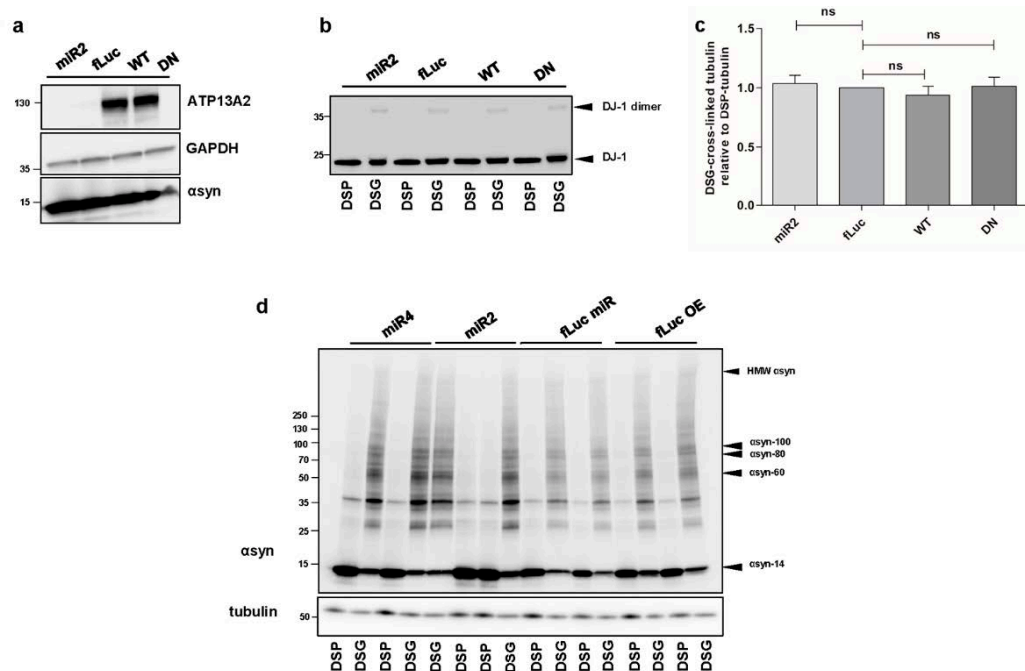


Figure A1. (a) Visualization of ATP13A2 and αsyn levels in ATP13A2 KD, fLuc, ATP13A2 WT, and ATP13A2 DN cells using GAPDH as a standard. (b) Visualization of DJ-1 dimers after cross-linking in ATP13A2 KD, fLuc, ATP13A2 WT, and ATP13A2 DN cells. (c) Quantification of the ratio of DSG cross-linked tubulin (~55 kDa) to DSP tubulin (~55 kDa) in the ATP13A2 KD, ATP13A2 WT, and ATP13A2 DN cells relative to the ratio in the control cells ($n = 4$). Statistical analysis was performed using a one-way ANOVA test with Bonferroni. The error bars represent the SEM. ns, not significant. (d) Visualization of αsyn multimers after cross-linking in ATP13A2 miR4 (a second ATP13A2 sh sequence), ATP13A2 miR2, fLuc miR, and fLuc overexpression cells.

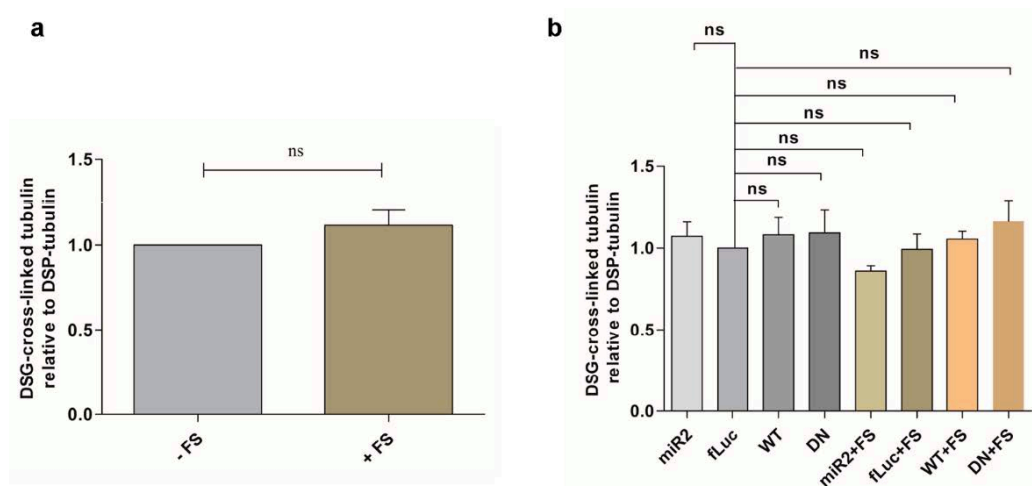


Figure A2. (a) Quantification of ratio of DSG cross-linked tubulin (~55 kDa) to DSP tubulin (~55 kDa) in oxidative stress-treated fLuc cells relative to the ratio in the control cells ($n = 3$). Statistical analysis was performed with column statistics (one-sample t -test) comparing test values to the hypothetical value of 1. The error bars represent the SEM. ns, not significant. (b) Quantification of ratio of DSG cross-linked tubulin (~55 kDa) to DSP tubulin (~55 kDa) in ATP13A2 KD, fLuc, ATP13A2 WT, and ATP13A2 DN cells without or with oxidative stress relative to the ratio in the control fLuc cells ($n = 3$). Statistical analysis was performed using a one-way ANOVA test with Bonferroni. The error bars represent the SEM. ns, not significant.

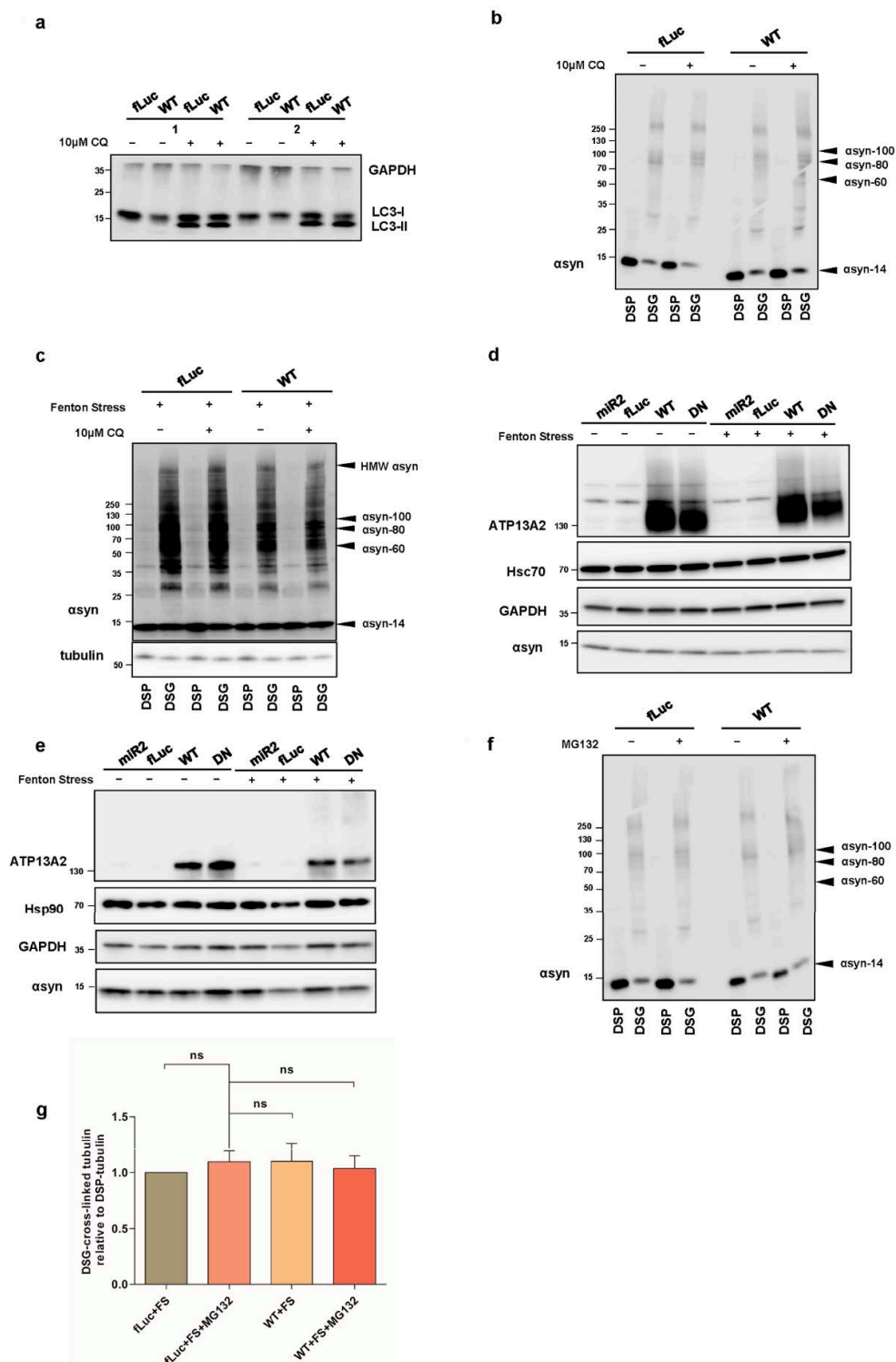


Figure A3. (a) Visualization of microtubule-associated protein 1A/1B-light chain 3 (LC3)-I and LC3-II levels in fLuc and ATP13A2 WT cells treated with or without CQ using GAPDH as a standard. (b) Visualization of αsyn multimers after cross-linking in fLuc and ATP13A2 WT cells treated with or without CQ. (c) Visualization of αsyn multimers after cross-linking in fLuc and ATP13A2 WT cells treated with oxidative stress combined with or without CQ. Visualization of heat shock cognate 71 kDa protein (Hsc70) (d) and heat shock protein 90 (Hsp90) (e) in ATP13A2 KD, fLuc, ATP13A2 WTm and ATP13A2 DN cells with or without oxidative stress. (f) Visualization of αsyn multimers after cross-linking in fLuc and ATP13A2 WT treated with or without MG132. (g) Quantification of ratio of DSG cross-linked tubulin (~55 kDa) to DSP tubulin (~55 kDa) relative to the ratio in the control fLuc cells ($n = 3$). Statistical analysis was performed using a one-way ANOVA test with Bonferroni. The error bars represent the SEM. ns, not significant.

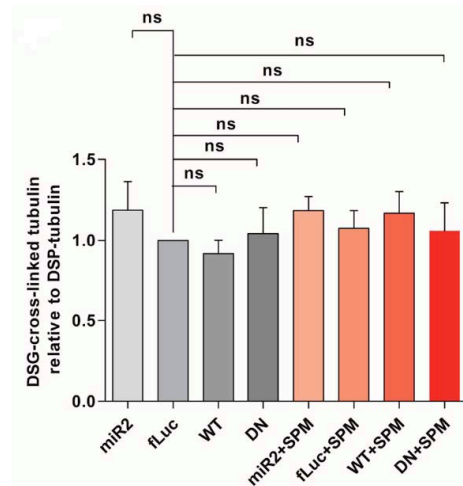


Figure A4. Quantification of ratio of DSG cross-linked tubulin (~55 kDa) to DSP tubulin (~55 kDa) in SPM-treated cells relative to the ratio in the untreated control cells ($n = 3$). Statistical analysis was performed using a one-way ANOVA test with Bonferroni. The error bars represent the SEM. ns, not significant.

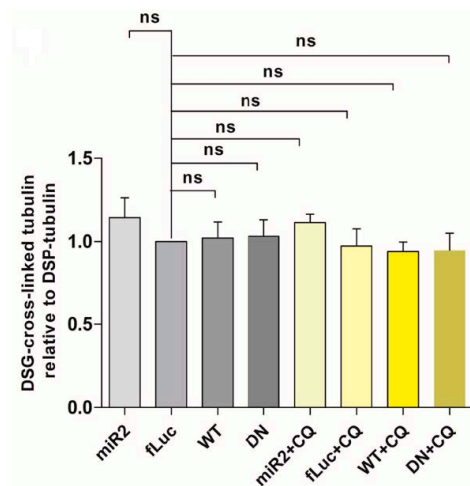


Figure A5. Quantification of ratio of DSG cross-linked tubulin (~55 kDa) to DSP tubulin (~55 kDa) relative to the ratio in the control fLuc cells ($n = 3$). Statistical analysis was performed using a one-way ANOVA test with Bonferroni. The error bars represent the SEM. ns, not significant.

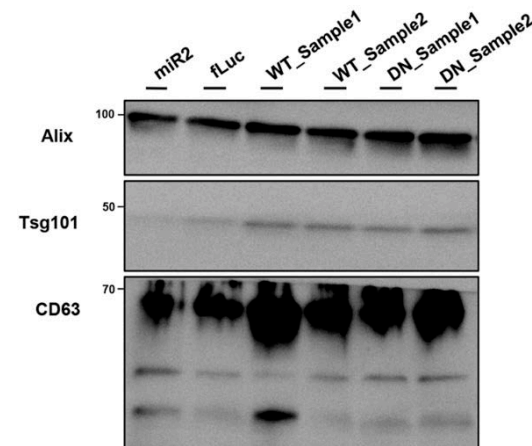


Figure A6. Visualization of exosome marker proteins (Alix, Tsg101, and CD63) in nanovesicles from ATP13A2 KD, fLuc, ATP13A2 WT, and ATP13A2 DN cells.

References

1. Kalia, L.V.; Lang, A.E. Parkinson's disease. *Lancet* **2015**, *386*, 896–912. [[CrossRef](#)]
2. Armstrong, M.J.; Okun, M.S. Diagnosis and Treatment of Parkinson Disease: A Review. *JAMA* **2020**, *323*, 548–560. [[CrossRef](#)]
3. Spillantini, M.G.; Schmidt, M.L.; Lee, V.M.Y.; Trojanowski, J.Q.; Jakes, R.; Goedert, M. α -Synuclein in Lewy bodies. *Nature* **1997**, *388*, 839–840. [[CrossRef](#)] [[PubMed](#)]
4. Goedert, M.; Spillantini, M.G.; Del Tredici, K.; Braak, H. 100 years of Lewy pathology. *Nat. Rev. Neurol.* **2013**, *9*, 12. [[CrossRef](#)] [[PubMed](#)]
5. Deng, H.; Wang, P.; Jankovic, J. The genetics of Parkinson disease. *Ageing Res. Rev.* **2018**, *42*, 72–85. [[CrossRef](#)]
6. Wong, Y.C.; Krainc, D. α -synuclein toxicity in neurodegeneration: Mechanism and therapeutic strategies. *Nat. Med.* **2017**, *23*, 1–13. [[CrossRef](#)]
7. Boassa, D.; Berlanga, M.L.; Yang, M.A.; Terada, M.; Hu, J.; Bushong, E.A.; Hwang, M.; Masliah, E.; George, J.M.; Ellisman, M.H. Mapping the subcellular distribution of α -synuclein in neurons using genetically encoded probes for correlated light and electron microscopy: Implications for Parkinson's disease pathogenesis. *J. Neurosci.* **2013**, *33*, 2605–2615. [[CrossRef](#)]
8. Burré, J.; Sharma, M.; Südhof, T.C. Cell Biology and Pathophysiology of α -Synuclein. *Cold Spring Harb. Perspect. Med.* **2018**, *8*, a024091. [[CrossRef](#)]
9. Emanuele, M.; Chieregatti, E. Mechanisms of alpha-synuclein action on neurotransmission: Cell-autonomous and non-cell autonomous role. *Biomolecules* **2015**, *5*, 865–892. [[CrossRef](#)]
10. Lee, H.-J.; Choi, C.; Lee, S.-J. Membrane-bound alpha-synuclein has a high aggregation propensity and the ability to seed the aggregation of the cytosolic form. *J. Biol. Chem.* **2002**, *277*, 671–678. [[CrossRef](#)]
11. Necula, M.; Chirita, C.N.; Kuret, J. Rapid Anionic Micelle-mediated α -Synuclein Fibrillization in Vitro. *J. Biol. Chem.* **2003**, *278*, 46674–46680. [[CrossRef](#)] [[PubMed](#)]
12. Macchi, F.; Deleersnijder, A.; Van den Haute, C.; Munck, S.; Pottel, H.; Michiels, A.; Debysere, Z.; Gerard, M.; Baekelandt, V. High-content analysis of α -synuclein aggregation and cell death in a cellular model of Parkinson's disease. *J. Neurosci. Methods* **2015**, *261*, 1–11. [[CrossRef](#)]
13. Mehra, S.; Sahay, S.; Maji, S.K. α -Synuclein misfolding and aggregation: Implications in Parkinson's disease pathogenesis. *Biochim. Biophys. Acta Proteins Proteom.* **2019**, *1867*, 890–908. [[CrossRef](#)]
14. Ramirez, A.; Heimbach, A.; Gründemann, J.; Stiller, B.; Hampshire, D.; Cid, L.P.; Goebel, I.; Mubaidin, A.F.; Wriekat, A.-L.; Roeper, J.; et al. Hereditary parkinsonism with dementia is caused by mutations in ATP13A2, encoding a lysosomal type 5 P-type ATPase. *Nat. Genet.* **2006**, *38*, 1184–1191. [[CrossRef](#)]
15. Kong, S.M.; Chan, B.K.; Park, J.-S.; Hill, K.J.; Aitken, J.B.; Cottle, L.; Farghaian, H.; Cole, A.R.; Lay, P.A.; Sue, C.M.; et al. Parkinson's disease-linked human PARK9/ATP13A2 maintains zinc homeostasis and promotes α -Synuclein externalization via exosomes. *Hum. Mol. Genet.* **2014**, *23*, 2816–2833. [[CrossRef](#)] [[PubMed](#)]
16. Eiberg, H.; Hansen, L.; Korbo, L.; Nielsen, I.; Svenstrup, K.; Bech, S.; Pinborg, L.; Friberg, L.; Hjerminde, L.; Olsen, O.; et al. Novel mutation in ATP13A2 widens the spectrum of Kufor-Rakeb syndrome (PARK9). *Clin. Genet.* **2011**, *82*, 256–263. [[CrossRef](#)]
17. Podhajski, A.; Musso, A.; Trancikova, A.; Stafa, K.; Moser, R.; Sonnay, S.; Glauser, L.; Moore, D.J. Common Pathogenic Effects of Missense Mutations in the P-Type ATPase ATP13A2 (PARK9) Associated with Early-Onset Parkinsonism. *PLoS ONE* **2012**, *7*, e39942. [[CrossRef](#)]
18. Jamil, M.; Siddiqui, A.W.; Sollinger, A.; Ferrara, J. ATP13A2-Related Hereditary Spastic Paraplegia (HSP) (P6.044). *Neurology* **2018**, *90*, P6.044.
19. Bras, J.; Verloes, A.; Schneider, S.A.; Mole, S.E.; Guerreiro, R.J. Mutation of the parkinsonism gene ATP13A2 causes neuronal ceroid-lipofuscinosis. *Hum. Mol. Genet.* **2012**, *21*, 2646–2650. [[CrossRef](#)] [[PubMed](#)]
20. Spataro, R.; Kousi, M.; Farhan, S.M.K.; Willer, J.R.; Ross, J.P.; Dion, P.A.; Rouleau, G.A.; Daly, M.J.; Neale, B.M.; La Bella, V.; et al. Mutations in ATP13A2 (PARK9) are associated with an amyotrophic lateral sclerosis-like phenotype, implicating this locus in further phenotypic expansion. *Hum. Genom.* **2019**, *13*, 1–10. [[CrossRef](#)]
21. Usenovic, M.; Tresse, E.; Mazzulli, J.R.; Taylor, J.P.; Krainc, D. Deficiency of ATP13A2 leads to lysosomal dysfunction, α -synuclein accumulation, and neurotoxicity. *J. Neurosci.* **2012**, *32*, 4240–4246. [[CrossRef](#)]
22. Matsui, H.; Sato, F.; Sato, S.; Koike, M.; Taruno, Y.; Saiki, S.; Funayama, M.; Ito, H.; Taniguchi, Y.; Uemura, N.; et al. ATP13A2 deficiency induces a decrease in cathepsin D activity, fingerprint-like inclusion body formation, and selective degeneration of dopaminergic neurons. *FEBS Lett.* **2013**, *587*, 1316–1325. [[CrossRef](#)]
23. Grünewald, A.; Arns, B.; Seibler, P.; Rakovic, A.; Münchau, A.; Ramirez, A.; Sue, C.M.; Klein, C. ATP13A2 mutations impair mitochondrial function in fibroblasts from patients with Kufor-Rakeb syndrome. *Neurobiol. Aging* **2012**, *33*, 1843.e1–1843.e7.
24. Gusdon, A.M.; Zhu, J.; Van Houten, B.; Chu, C.T. ATP13A2 regulates mitochondrial bioenergetics through macroautophagy. *Neurobiol. Dis.* **2012**, *45*, 962–997. [[CrossRef](#)]
25. Park, J.-S.; Koentjoro, B.; Veivers, D.; Mackay-Sim, A.; Sue, C.M. Parkinson's disease-associated human ATP13A2 (PARK9) deficiency causes zinc dyshomeostasis and mitochondrial dysfunction. *Hum. Mol. Genet.* **2014**, *23*, 2802–2815. [[CrossRef](#)] [[PubMed](#)]
26. Schultheis, P.J.; Fleming, S.M.; Clippinger, A.K.; Lewis, J.; Tsunemi, T.; Giasson, B.; Dickson, D.W.; Mazzulli, J.R.; Bardgett, M.E.; Haik, K.L.; et al. Atp13a2-deficient mice exhibit neuronal ceroid lipofuscinosis, limited α -synuclein accumulation and age-dependent sensorimotor deficits. *Hum. Mol. Genet.* **2013**, *22*, 2067–2082. [[CrossRef](#)]

27. Tsunemi, T.; Hamada, K.; Krainc, D. ATP13A2/PARK9 Regulates Secretion of Exosomes and α -Synuclein. *J. Neurosci.* **2014**, *34*, 15281–15287. [[CrossRef](#)] [[PubMed](#)]
28. Gitler, A.D.; Chesi, A.; Geddie, M.L.; Strathearn, K.E.; Hamamichi, S.; Hill, K.J.; Caldwell, K.A.; Caldwell, G.A.; Cooper, A.A.; Rochet, J.-C.; et al. Alpha-synuclein is part of a diverse and highly conserved interaction network that includes PARK9 and manganese toxicity. *Nat. Genet.* **2009**, *41*, 308–315. [[CrossRef](#)]
29. Dirr, E.R.; Ekhtor, O.R.; Blackwood, R.; Holden, J.G.; Masliah, E.; Schultheis, P.J.; Fleming, S.M. Exacerbation of sensorimotor dysfunction in mice deficient in Atp13a2 and overexpressing human wildtype alpha-synuclein. *Behav. Brain Res.* **2018**, *343*, 41–49. [[CrossRef](#)] [[PubMed](#)]
30. Kett, L.R.; Stiller, B.; Bernath, M.M.; Tasset, I.; Blesa, J.; Jackson-Lewis, V.; Chan, R.B.; Zhou, B.; Paolo, G.D.; Przedborski, S.; et al. α -Synuclein-Independent Histopathological and Motor Deficits in Mice Lacking the Endolysosomal Parkinsonism Protein Atp13a2. *J. Neurosci.* **2015**, *35*, 5724–5742. [[CrossRef](#)]
31. Daniel, G.; Musso, A.; Tsika, E.; Fiser, A.; Glauser, L.; Pletnikova, O.; Schneider, B.L.; Moore, D.J. α -Synuclein-induced dopaminergic neurodegeneration in a rat model of Parkinson's disease occurs independent of ATP13A2 (PARK9). *Neurobiol. Dis.* **2015**, *73*, 229–243. [[CrossRef](#)]
32. van Veen, S.; Martin, S.; Van den Haute, C.; Benoy, V.; Lyons, J.; Vanhoutte, R.; Kahler, J.P.; Decuyper, J.-P.; Gelders, G.; Lambie, E.; et al. ATP13A2 deficiency disrupts lysosomal polyamine export. *Nature* **2020**, *578*, 419–424. [[CrossRef](#)]
33. Igarashi, K.; Kashiwagi, K. Modulation of cellular function by polyamines. *Int. J. Biochem. Cell Biol.* **2010**, *42*, 39–51. [[CrossRef](#)]
34. Pegg, A.E. Functions of Polyamines in Mammals. *J. Biol. Chem.* **2016**, *291*, 14904–14912. [[CrossRef](#)]
35. Vrijisen, S.; Besora-Casals, L.; Van Veen, S.; Zielich, J.; Haute, C.V.D.; Hamouda, N.N.; Fischer, C.; Ghesquière, B.; Tournev, I.; Agostinis, P.; et al. ATP13A2-mediated endo-lysosomal polyamine export counters mitochondrial oxidative stress. *Proc. Natl. Acad. Sci. USA* **2020**, *117*, 31198–31207. [[CrossRef](#)]
36. Grabenauer, M.; Bernstein, S.L.; Lee, J.C.; Wyttenbach, T.; Dupuis, N.F.; Gray, H.B.; Winkler, J.R.; Bowers, M.T. Spermine Binding to Parkinson's Protein α -Synuclein and Its Disease-Related A30P and A53T Mutants. *J. Phys. Chem. B* **2008**, *112*, 11147–11154. [[CrossRef](#)] [[PubMed](#)]
37. Krasnoslobodtsev, A.V.; Peng, J.; Asiago, J.M.; Hindupur, J.; Rochet, J.-C.; Lyubchenko, Y.L. Effect of Spermidine on Misfolding and Interactions of Alpha-Synuclein. *PLoS ONE* **2012**, *7*, e38099. [[CrossRef](#)] [[PubMed](#)]
38. Xilouri, M.; Brekk, O.R.; Stefanis, L. Alpha-synuclein and Protein Degradation Systems: A Reciprocal Relationship. *Mol. Neurobiol.* **2013**, *47*, 537–551. [[CrossRef](#)] [[PubMed](#)]
39. Lopes da Fonseca, T.; Pinho, R.; Outeiro, T.F. A familial ATP13A2 mutation enhances alpha-synuclein aggregation and promotes cell death. *Hum. Mol. Genet.* **2016**, *25*, 2959–2971. [[CrossRef](#)] [[PubMed](#)]
40. Dettmer, U.; Newman, A.J.; Luth, E.S.; Bartels, T.; Selkoe, D. In Vivo Cross-linking Reveals Principally Oligomeric Forms of α -Synuclein and β -Synuclein in Neurons and Non-neural Cells. *J. Biol. Chem.* **2013**, *288*, 6371–6385. [[CrossRef](#)] [[PubMed](#)]
41. Schuber, F. Influence of polyamines on membrane functions. *Biochem. J.* **1989**, *260*, 1–10. [[CrossRef](#)] [[PubMed](#)]
42. Demirsoy, S.; Martin, S.; Motamedi, S.; van Veen, S.; Holemans, T.; Van den Haute, C.; Jordanova, A.; Baekelandt, V.; Vangheluwe, P.; Agostinis, P. ATP13A2/PARK9 regulates endo-/lysosomal cargo sorting and proteostasis through a novel PI(3, 5)P2-mediated scaffolding function. *Hum. Mol. Genet.* **2017**, *26*, 1656–1669. [[CrossRef](#)] [[PubMed](#)]
43. Antony, T.; Hoyer, W.; Cherny, D.; Heim, G.; Jovin, T.M.; Subramaniam, V. Cellular Polyamines Promote the Aggregation of α -Synuclein. *J. Biol. Chem.* **2003**, *278*, 3235–3240. [[CrossRef](#)] [[PubMed](#)]
44. Tsigelny, I.F.; Sharikov, Y.; Wrasidlo, W.; Gonzalez, T.; Desplats, P.A.; Crews, L.; Spencer, B.; Masliah, E. Role of α -synuclein penetration into the membrane in the mechanisms of oligomer pore formation. *FEBS J.* **2012**, *279*, 1000–1013. [[CrossRef](#)]
45. Auluck, P.K.; Caraveo, G.; Lindquist, S. α -Synuclein: Membrane interactions and toxicity in Parkinson's disease. *Annu. Rev. Cell Dev. Biol.* **2010**, *26*, 211–233. [[CrossRef](#)]
46. Tsunemi, T.; Krainc, D. Zn²⁺ dyshomeostasis caused by loss of ATP13A2/PARK9 leads to lysosomal dysfunction and alpha-synuclein accumulation. *Hum. Mol. Genet.* **2014**, *23*, 2791–2801. [[CrossRef](#)] [[PubMed](#)]
47. Holemans, T.; Sørensen, D.M.; van Veen, S.; Martin, S.; Hermans, D.; Kemmer, G.C.; Van den Haute, C.; Baekelandt, V.; Pomorski, T.G.; Agostinis, P.; et al. A lipid switch unlocks Parkinson's disease-associated ATP13A2. *Proc. Natl. Acad. Sci. USA* **2015**, *112*, 9040–9045. [[CrossRef](#)] [[PubMed](#)]